Analysis of $C_2H_4O_2$ Isomers in NGC 6334 I

Samer El-Abd

Advisor: Crystal Brogan

May 8th, 2018

Department of Astronomy

University of Virginia

This thesis is submitted in partial completion of the requirements of the BS Astronomy-Physics Major

Draft version May 8, 2018
Preprint typeset using LaTeX style emulateapj v. 01/23/15

ANALYSIS OF $C_2H_4O_2$ ISOMERS IN NGC 6334 I

S. J. El-Abd[1], C. L. Brogan[2], T. R. Hunter[2], B. A. McGuire[2]

Draft version May 8, 2018

ABSTRACT

We have analyzed the abundances of the three isomers methyl formate (CH_3OCHO), glycolaldehyde (cis-CH_2OHCHO), and acetic acid (CH_3COOH) in the NGC 6334 I-MM1 and -MM2 massive star-forming regions using Atacama Large Millimeter/submillimeter Array (ALMA) data. In the MM1 star-forming region, we derived column densities of $9.93(94)\times10^{17}$ cm^{-2} for methyl formate, $1.24(16)\times10^{17}$ cm^{-2} for acetic acid, and $9.31(68)\times10^{15}$ cm^{-2} for glycolaldehyde. In the MM2 star-forming region we derived column densities of $9(1)\times10^{18}$ cm^{-2} for methyl formate and $1.48(25)\times10^{17}$ cm^{-2} for acetic acid. An upper limit of 1.15×10^{16} cm^{-2} was calculated for the column density of glycolaldehyde in MM2. These abundances are compared to other star-forming regions and theories on the chemical reasons for their differences are presented.

Keywords: stars: massive — astrochemistry: individual(NGC 6334 I)

1. INTRODUCTION

In contrast to their low mass counterparts, the mechanisms by which massive stars are formed are still relatively poorly understood. NGC 6334 I is one of the nearest massive star-forming regions at 1.3 kpc away (Reid et al. 2014); this makes it a prime candidate for spectroscopic observations to constrain the chemical makeup of its composite star-forming regions. Our observations were centered on the NGC 6334 I-MM1 and -MM2 star-forming regions, separated by about 3″ (4000 au; Figure 1); MM1 and MM2 refer to the regions as they are named in Brogan et al. (2016). The small separation between these two regions means that their composition was most likely similar when they began collapsing to form stars. This removes a significant variable when comparing the progression of these regions; differences in their evolution can then be more concretely attributed to measurable physical conditions.

The formation of complex organic molecules (COMs), those species with 5 or more atoms (Herbst & van Dishoeck 2009), is a phenomenon that is well suited for study in the early stages of massive star formation. Many of the radicals which drive the production of these COMs - methyl (CH_3), hydroxymethyl (CH_2OH), and methoxy (CH_3O) - are produced during the photodissociation of methanol (CH_3OH) on grain surfaces (Laas et al. 2011). The ratios at which these radicals are produced influences the relative abundances of the COMs they form. This is especially relevant to a molecule as abundant in star-forming regions as methyl formate and its isomers, acetic acid and glycolaldehyde. The relative abundances of these three isomers can point to formation pathways which in turn can further illuminate the chemical processes happening in these dense clouds.

2. OBSERVATIONS

The ALMA data that were used for this analysis were observed during Cycle 3 in 2016, project code 2015.A.00022.T. The data were calibrated using the ALMA cycle 4 pipeline (CASA 4.7.2); for further information refer to Hunter et al. (2017). The observation was centered at (J2000 17:20:53.36, -35:47:00.0) and had a nominal resolution of $0.24''\times0.17''$ ($-83°$), a full width half-power (FWHP) of the primary beam of 20″, a spectral resolution of 1.1 km s^{-1}, and a rms per channel of 2.0 mJy beam^{-1} (0.62 K). The observations consisted of two tunings, each with four spectral windows, with a bandwidth of 1.87 GHz per window. The first set of spectral windows were centered at 280.1, 282.0, 292.1, and 294.0 GHz. The second set of spectral windows were centered at 337.1, 339.0, 349.1, and 351.0 GHz. Primary beam corrections were applied to the images before analysis.

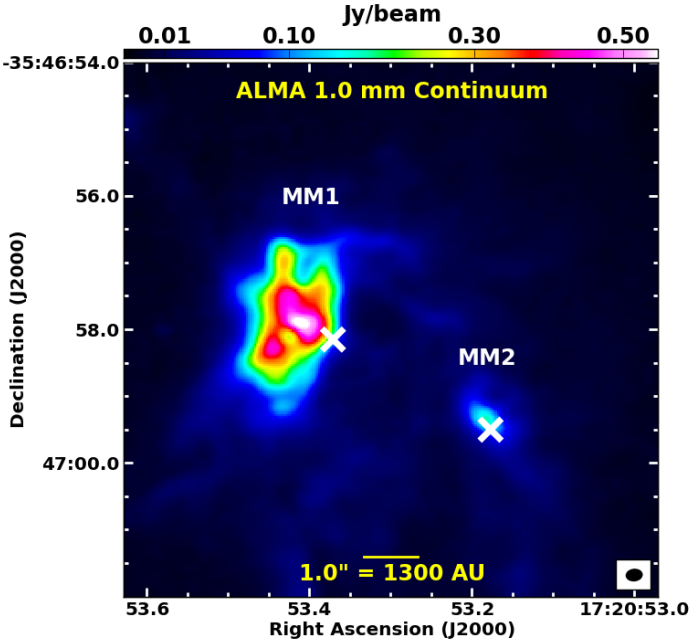

Figure 1. Image of the ALMA 1 mm continuum emission toward NGC 6334 I-MM1 and MM2 from Hunter et al. (2017). The positions of the spectra analyzed for MM1 and MM2 are shown with white crosses. The continuum synthesized beam of $0.''24\times0.''17$, PA= $-83°$ is shown in the lower right.

[1] Department of Astronomy, University of Virginia, P.O. Box 3818, Charlottesville, VA 22903, USA
[2] NRAO, 520 Edgemont Rd, Charlottesville, VA 22903, USA

Further details are given in McGuire et al. (2017) and Hunter et al. (2017).

3. ANALYSIS

The analysis was carried out on spectra extracted from (J2000 17:20:53.373, -35:46:58.14) for the MM1 region and (J2000 17:20:53.1776, -35:46:59.490) for the MM2 region (see Fig. 1). These positions were intentionally offset from the bright continuum peaks to avoid effects from the high continuum opacity (spectral absorption and attenuation). We began analyzing these spectra by building a simulated model of the observed line emission from molecules at local thermodynamic equilibrium (LTE). The LTE assumption meant that the excitation temperature of the lines was dominated by molecular collisions rather than radiative processes; this was checked by calculating the critical density, n_{cr}, of representative transitions of the COMs, using

$$n_{cr} = \frac{A_{ul}}{\gamma_{ul}}, \tag{1}$$

where A_{ul} is the Einstein A coefficient (s^{-1}) and γ_{ul} is the collisional rate coefficient ($cm^3\ s^{-1}$). As the rate coefficients for the $C_2H_4O_2$ isomers are unavailable, the critical density for each molecule was calculated using the coefficients for analogous transitions of methanol, which is the most similar molecule for which the coefficients are available (Rabli et al. 2010). Using this method, the critical density was estimated to be between $10^5 - 10^6$ cm^{-3}. The average density throughout the entire cloud was calculated to be 1.5×10^5 cm^{-3} in Russeil et al. (2010); the density in the targeted cores is much greater than the density averaged over the entire cloud, so the LTE assumption is valid. The distribution of energy levels for the molecules is then given by a Boltzmann distribution at the excitation temperature, T_{ex}, which is a measure of the ratio of molecules in the upper and lower states. The excitation temperature was calculated by adding the background temperature to the intensity of the optically thick lines, using the relation given in Turner (1991)

$$\Delta T_B = [J_\nu(T_{ex}) - J_\nu(T_{bg})](1 - e^{-\tau_0}), \tag{2}$$

where

$$J_\nu(T) \equiv (h\nu/k)[exp(h\nu/kT) - 1]^{-1}. \tag{3}$$

The model was built by simulating the spectrum of one molecule at a time and changing the temperature, linewidth, and column density for each molecule to best fit the observed data; this was done for 78 common interstellar molecules, not all of which were present. The spectral line properties for all of the simulated molecules were obtained from the Splatalogue database. With the model built, the three structural isomers methyl formate, acetic acid, and glycolaldehyde were chosen for further analysis in an attempt to constrain the chemical processes in each region. The molecular line properties of the $C_2H_4O_2$ isomers were obtained from Ilyushin et al. (2009), Ilyushin et al. (2013), and Carroll et al. (2010), respectively. The composite spectral line model allowed for the identification of unblended lines in the sources for the three isomers. Figures A1-16 show the model spectra for MM1 and MM2.

The first attempt at calculating the column densities was done with a rotation diagram following the methods of Goldsmith & Langer (1999). The rotation diagram was created by manipulating Equation 4 such that the natural log of the integrated intensity, multiplied by the constants in the equation, could be plotted versus the upper state energy for each transition. Provided the chosen transitions are optically thin and in LTE, the points should then lie on a straight line where the negative inverse of the slope yields the excitation temperature and the natural log of the column density is proportional to the y-intercept. While this method produced acceptable results for methyl formate in MM1, there were many outlying points on the rotation diagrams for the other molecules. This is likely due to the fact that lines that previously appeared to be unblended were in fact overlapping with lines from molecules that were not simulated.

Instead, to calculate the column densities we selected the least blended transitions for each molecule in MM1 and MM2. A least-squares fit of the column density for these unblended lines to best match the intensities of the observed transitions. Observed lines that greatly disagreed with the simulation after the fit were discarded as they were likely blended with molecules that weren't in the model. The simulated transition that best matched the intensity of the observed transition after the least-squares fit was chosen to be an accurate measure of the abundance of the molecule using Equation 4.

$$N_T = \frac{1}{2}\frac{3k}{8\pi^3}\sqrt{\frac{\pi}{\ln 2}}\frac{Qe^{E_u/T_{ex}}\Delta T_b \Delta V}{\nu S\mu^2\eta_B}\frac{1}{1 - \frac{e^{h\nu/kT_{ex}}-1}{e^{h\nu/kT_{bg}}-1}} \tag{4}$$

Here, Q is the partition function, E_u is the upper state energy, ΔT_b is the brightness temperature, ΔV is the linewidth, S is the intrinsic line strength, μ^2 is the transition dipole moment, η_B is the efficiency of the beam, and T_{bg} is the background temperature. The partition function was calculated through a direct summation of states as described in Gordy & Cook (1984).

The selected transitions for each molecule in MM1 and MM2 can be seen in Tables 1 and 2, respectively. However, a confident claim for the detection of glycolaldehyde in MM2 could not be made; the upper limit given in Table 2 was calculated by finding the strongest line of glycolaldehyde that was undetected and recording the intensity of the observed spectrum at that point.

4. RESULTS AND DISCUSSION

The derived column densities for the three $C_2H_4O_2$ isomers in NGC 6334 I-MM1 and NGC 6334 I-MM2 are presented in Table 3. As can be seen in Figure 2, the comparative abundance of methyl formate to acetic acid in MM2 is nearly an order of magnitude higher than that in MM1. The non-detection of glycolaldehyde in MM2 makes it impossible to draw concrete conclusions on its comparative abundance between the two sources. Even so, at minimum, the comparative abundance of methyl formate to glycolaldehyde in MM2 is also nearly an order of magnitude greater than in MM1. It can also be seen that the excitation temperature of the two sources are very close, with MM1 being the slightly cooler of the two sources. It should be noted that the excitation temperature derived for MM1 is likely not truly representative

Table 1
Transitions Used to Calculate Column Densities in NGC 6334 I-MM1

Molecule	$J'_{K_a,K_c} \rightarrow J''_{K_a,K_c}$	A/E	Frequency (MHz)	T_B (K)	ΔV (km s^{-1})	$S_{ij}\mu^2$ (D^2)	E_{upper} (K)
Methyl formate	$28_{8,20} \rightarrow 27_{8,19}$	A	351842.1930	77.10	2.4	68.60	284.087
Acetic Acid	$23_{3,20} \rightarrow 22_{3,19}$	E	279775.7200	37.13	2.4	111.5	177.856
Glycolaldehyde	$16_{7,10} \rightarrow 15_{6,9}$		348314.0541	65.94	2.4	372.4	105.439

Table 2
Transitions Used to Calculate Column Densities in NGC 6334 I-MM2

Molecule	$J'_{K_a,K_c} \rightarrow J''_{K_a,K_c}$	A/E	Frequency (MHz)	T_B (K)	ΔV (km s^{-1})	$S_{ij}\mu^2$ (D^2)	E_{upper} (K)
Methyl Formate	$31_{11,20} \rightarrow 31_{10,21}$	E	280260.9740	37.77	2.4	5.92	373.984
Acetic Acid	$27_{x,27} \rightarrow 26_{x,26}$	A	292566.4000	59.33	2.4	153.4	199.743
Glycolaldehyde	$9_{8,x} \rightarrow 8_{7,x}$		293951.6852	8.90	2.4	42.5	63.86

Table 3
Properties of Each Molecule in MM1 and MM2

Molecule	Column Density (cm^{-2})	T_{ex} (K)	V_{LSR} (km s^{-1})
Methyl Formate (MM1)	$9.93 \pm 0.94 \times 10^{17}$	140	-7.00
Methyl Formate (MM2)	$9.32 \pm 1.00 \times 10^{18}$	152	-9.00
Acetic Acid (MM1)	$1.24 \pm 0.16 \times 10^{17}$	140	-7.00
Acetic Acid (MM2)	$1.48 \pm 0.25 \times 10^{17}$	152	-9.00
Glycolaldehyde (MM1)	$9.31 \pm 0.68 \times 10^{15}$	140	-7.00
Glycolaldehyde (MM2)	$< 1.15 \times 10^{16}$	152	...

of the nature of the source, as the extraction region for the spectral analysis was located further from the peak emission than the extraction region for MM2 in order to avoid absorption in the spectrum (Figure 1).

In Zernickel et al. (2012), the column density of methyl formate in NGC 6334 I was calculated using the *Herschel Space Observatory's* Heterodyne Instrument for the Far-Infrared (HIFI). The observation had a beam size ranging from 41″ to 12.5″, meaning that even with the minimum beam size it wouldn't be possible to differentiate the spectra of MM1 and MM2. Nevertheless, the column density derived in Zernickel et al. (2012) was comparable to the column density we derived in MM1, yet was about an order of magnitude less than that of MM2. The discrepancy in the column densities is likely due to the assumed source size used in Zernickel et al. (2012). A source size of 10″ was used, which is at least twice the size of the emitting region in Figure 1.

The relative abundances of methyl formate and its isomers in MM1 and MM2 are compared to the abundances in the star forming regions Orion-KL, Sgr B2(N), and IRAS 16293 in Figure 3. In each of the sources, a trend of methyl formate being more abundant than acetic acid, which in turn is more abundant than glycolaldehyde is noted; the exception to this is the source IRAS 16293. As the only low-mass star-forming region that is shown, IRAS 16293 provides a valuable point of comparison with respect to the other sources. The ratio of methyl formate to acetic acid in IRAS 16293 is in fact comparable to the ratio seen in the other high-mass star-forming regions; this makes the discrepancy in its glycolaldehyde abundance all the more curious. When comparing MM1 to the other massive star-forming regions, methyl formate is less abundant by about an order of magnitude relative to its isomers.

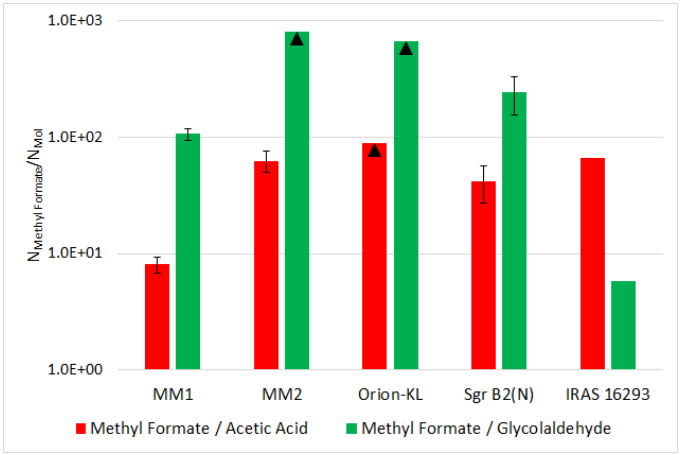

Figure 2. The relative abundances of methyl formate to acetic acid and glycolaldehyde in the star-forming regions NGC 6334 I-MM1, NGC 6334 I-MM2, Orion-KL (Favre et al. 2011), Sgr B2(N) (Belloche et al. 2013), and IRAS 16293 (Jørgensen et al. 2016). Errors were not available for the abundances in IRAS 16293.

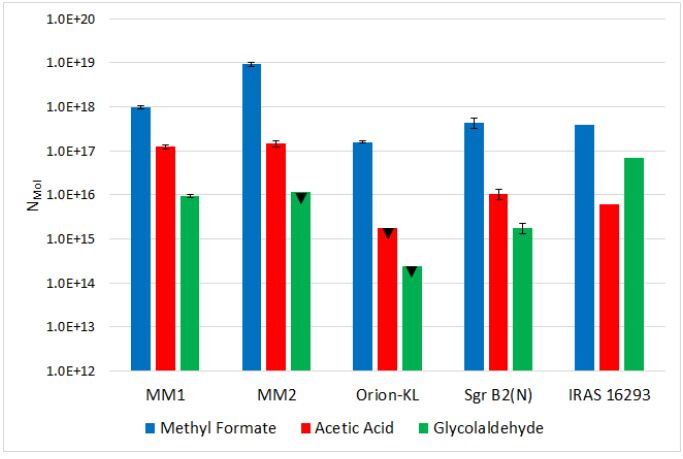

Figure 3. The observed abundances of methyl formate, acetic acid, and glycolaldehyde in the star-forming regions NGC 6334 I-MM1 and NGC 6334 I-MM2 from the current study, along with Orion-KL (Favre et al. 2011), Sgr B2(N) (Belloche et al. 2013), and IRAS 16293 (Jørgensen et al. 2016) for comparison.

Table 4
Ratio of Acetic Acid to Glycolaldehyde in Star-Forming Regions

Region	N_{AA} / N_G
MM1	13.3 ± 2.00
MM2	12.9 ± 2.18
Orion-KL	7.50^*
Sgr B2(N)	5.83 ± 2.06
IRAS 16293	0.09

* The ratio for Orion-KL was calculated using upper limits on the abundances of acetic acid and glycolaldehyde.

These molecules are largely produced in reactions that involve the methyl (CH_3), hydroxymethyl (CH_2OH), and methoxy (CH_3O) radicals (Laas et al. 2011). In Laas et al. (2011), which focused on the branching ratio of these radicals and their effect on the relative abundance of the three isomers analyzed in this work, the branching ratio which favored the production of the CH_3O radical was found to most accurately reproduce the abundances of methyl formate observed in Sgr B2(N). At the same time, increased production of the CH_3 radical provided marginally better agreement with the acetic acid and glycolaldehyde abundances. As the other massive star-forming regions are seen to produce similar ratios, it should be expected that a similar branching ratio is present in the sources, including NGC 6334 I. The overabundance of glycolaldehyde in the model of Laas et al. (2011) requires further analysis however.

In Table 4 it can be seen that the ratio of acetic acid to glycolaldehyde in each of the massive star-forming regions is remarkably similar (within a factor of 2), indicating the possibility of a common precursor molecule. Skouteris et al. (2018) showed that reactions of ethanol (CH_3CH_2OH) are capable of efficiently forming acetic acid and glycolaldehyde in the interstellar medium, and is possibly even a dominant formation pathway. The current observations certainly lend credence to the possibility. Further analysis on the ethanol content in each region is necessary to truly test whether it is in fact the precursor molecule to acetic acid and glycolaldehyde. In this case, the ethanol abundance in MM1 would be particularly enlightening; its ratio of acetic acid to glycolaldehyde is similar to the other massive star-forming regions, but acetic acid and glycolaldehyde are both more abundant by an order of magnitude relative to methyl formate in comparison to the other regions (Figure 2). The ethanol content in MM1 would then be an excellent indicator of the relationship between ethanol and acetic acid and glycolaldehyde; this will be followed up on in subsequent work. Another possibility for the disparity in MM1 abundances is that there is either some mechanism that is producing less methyl formate, or there is a destruction mechanism for methyl formate that is more prevalent than in other regions.

5. CONCLUSIONS

We have presented the abundances of the three $C_2H_4O_2$ isomers methyl formate, acetic acid, and glycolaldehyde in the massive star-forming region NGC 6334 I. These abundances were compared to the relative abundances in two other massive star-forming regions, Orion-KL and Sgr B2(N), as well as IRAS 16293, a low-mass star forming region. Distinct differences were present in the relative abundances of these isomers when comparing IRAS 16293 to the massive star-forming regions, indicating a a possible future avenue of study. A remarkably similar ratio of acetic acid to glycolaldehyde is noted in all of the massive star-forming regions. Our current theory is that this indicates a possible common precursor molecule, which could be ethanol, following the results of Skouteris et al. (2018). Measuring the ethanol abundance in these regions is a necessary step to test this theory, which will be carried out in subsequent work.

6. ACKNOWLEDGEMENTS

This paper makes use of the following ALMA data: ADS/JAO.ALMA#2015.A.00022.T ALMA is a partnership of ESO (representing its member states), NSF (USA) and NINS (Japan), together with NRC (Canada) and NSC and ASIAA (Taiwan) and KASI (Republic of Korea), in cooperation with the Republic of Chile. The Joint ALMA Observatory is operated by ESO, AUI/NRAO and NAOJ. The National Radio Astronomy Observatory is a facility of the National Science Foundation operated under cooperative agreement by Associated Universities, Inc. Support for B.A.M. was provided by NASA through Hubble Fellowship grant #HST-HF2-51396 awarded by the Space Telescope Science Institute, which is operated by the Association of Universities for Research in Astronomy, Inc., for NASA, under contract NAS5-26555.

REFERENCES

Belloche, A., Müller, H. S. P., Menten, K. M., Schilke, P., & Comito, C. 2013, A&A, 559, A47
Brogan, C. L., Hunter, T. R., Cyganowski, C. J., et al. 2016, ApJ, 832, 187
Carroll, P. B., Drouin, B. J., & Widicus Weaver, S. L. 2010, ApJ, 723, 845
Favre, C., Despois, D., Brouillet, N., et al. 2011, The Molecular Universe, 280, 156
Garrod, R. T., Widicus Weaver, S. L., & Herbst, E. 2008, ApJ, 682, 283-302
Goldsmith, P. F., & Langer, W. D. 1999, ApJ, 517, 209
Gordy W., Cook R. L., 1984, Microwave Molecular Spectra, 3 edn. Wiley, New York
Herbst, E., & van Dishoeck, E. F. 2009, ARA&A, 47, 427
Hunter, T. R., Brogan, C. L., MacLeod, G., et al. 2017, ApJL, 837, L29
Ilyushin, V., Kryvda, A., & Alekseev, E. 2009, Journal of Molecular Spectroscopy, 255, 32
Ilyushin, V. V., Endres, C. P., Lewen, F., Schlemmer, S., & Drouin, B. J. 2013, Journal of Molecular Spectroscopy, 290, 31
Jørgensen, J. K., van der Wiel, M. H. D., Coutens, A., et al. 2016, A&A, 595, A117
Laas, J. C., Garrod, R. T., Herbst, E., & Widicus Weaver, S. L. 2011, ApJ, 728, 71
McGuire, B. A., Shingledecker, C. N., Willis, E. R., et al. 2017, ApJL, 851, L46
Rabli, D., Flower, D.R. 2010, MNRAS 406, 95
Reid, M. J., Menten, K. M., Brunthaler, A., et al. 2014, ApJ, 783, 130
Remijan, A., Snyder, L. E., Friedel, D. N., Liu, S.-Y., & Shah, R. Y. 2003, ApJ, 590, 314
Russeil, D., Zavagno, A., Motte, F., et al. 2010, A&A, 515, A55
Skouteris, D., Balucani, N., Ceccarelli, C., et al. 2018, ApJ, 854, 135
Turner, B. E. 1991, ApJS, 76, 617
Zernickel, A., Schilke, P., Schmiedeke, A., et al. 2012, A&A, 546, A87

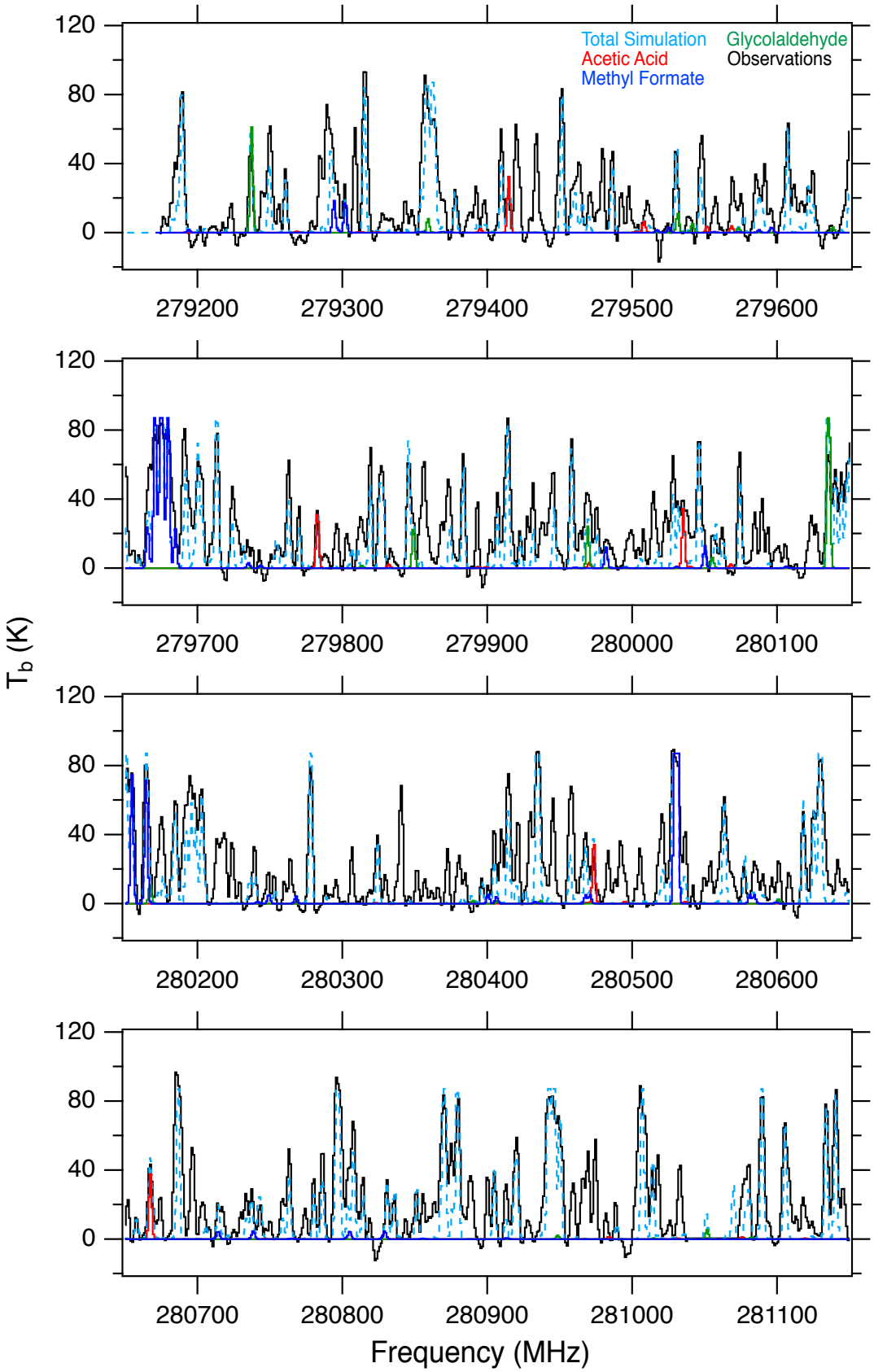

Figure A1. The simulated spectra for methyl formate, acetic acid, and glycolaldehyde are overlaid on the observed spectrum for MM1. The total simulation is also presented. For parameters on each of the fits refer to Table 3. The legend for the spectra is presented in the first panel.

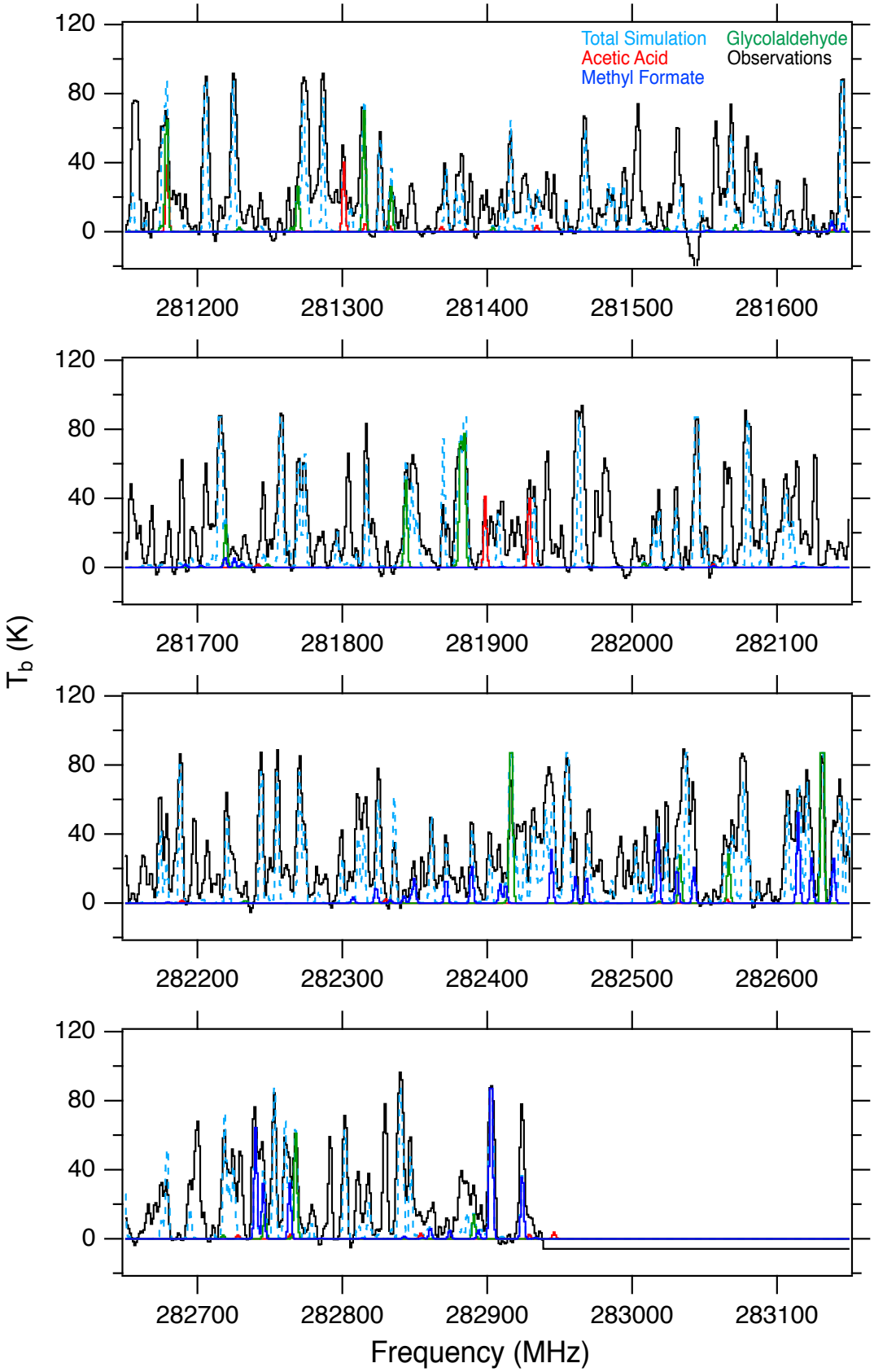

Figure A2. The simulated spectra for methyl formate, acetic acid, and glycolaldehyde are overlaid on the observed spectrum for MM1. The total simulation is also presented. For parameters on each of the fits refer to Table 3.

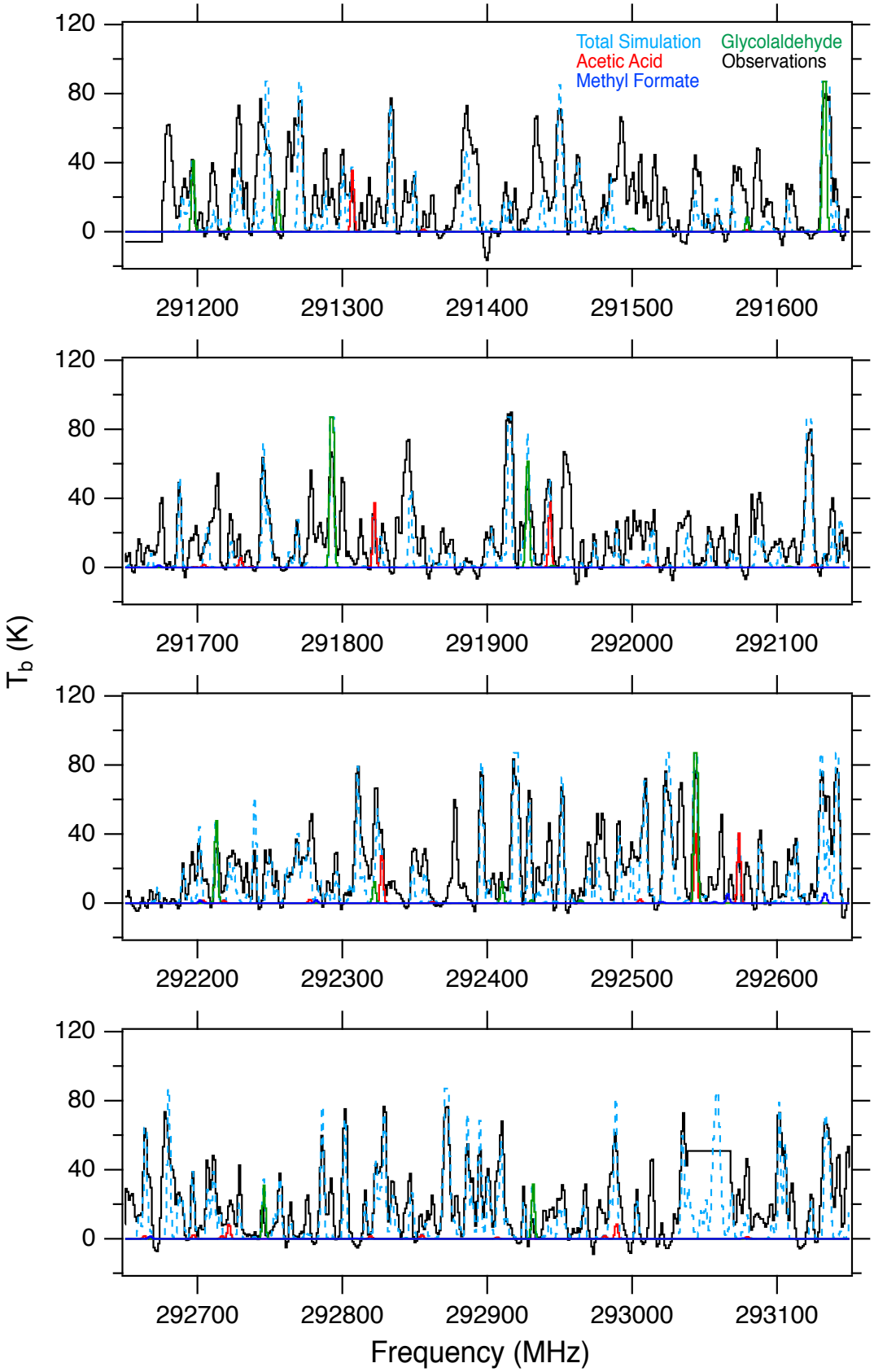

Figure A3. The simulated spectra for methyl formate, acetic acid, and glycolaldehyde are overlaid on the observed spectrum for MM1. The total simulation is also presented. For parameters on each of the fits refer to Table 3.

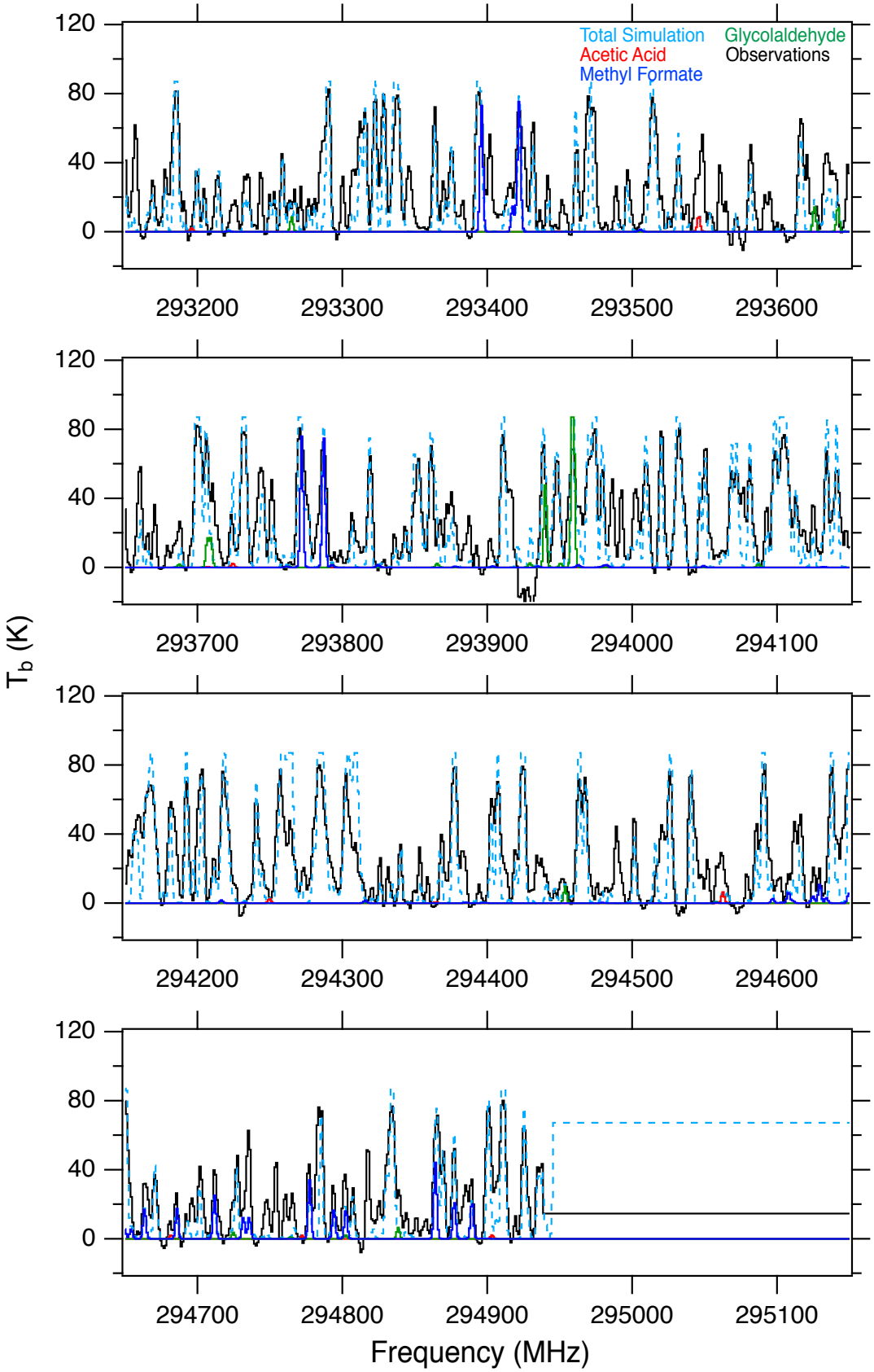

Figure A4. The simulated spectra for methyl formate, acetic acid, and glycolaldehyde are overlaid on the observed spectrum for MM1. The total simulation is also presented. For parameters on each of the fits refer to Table 3.

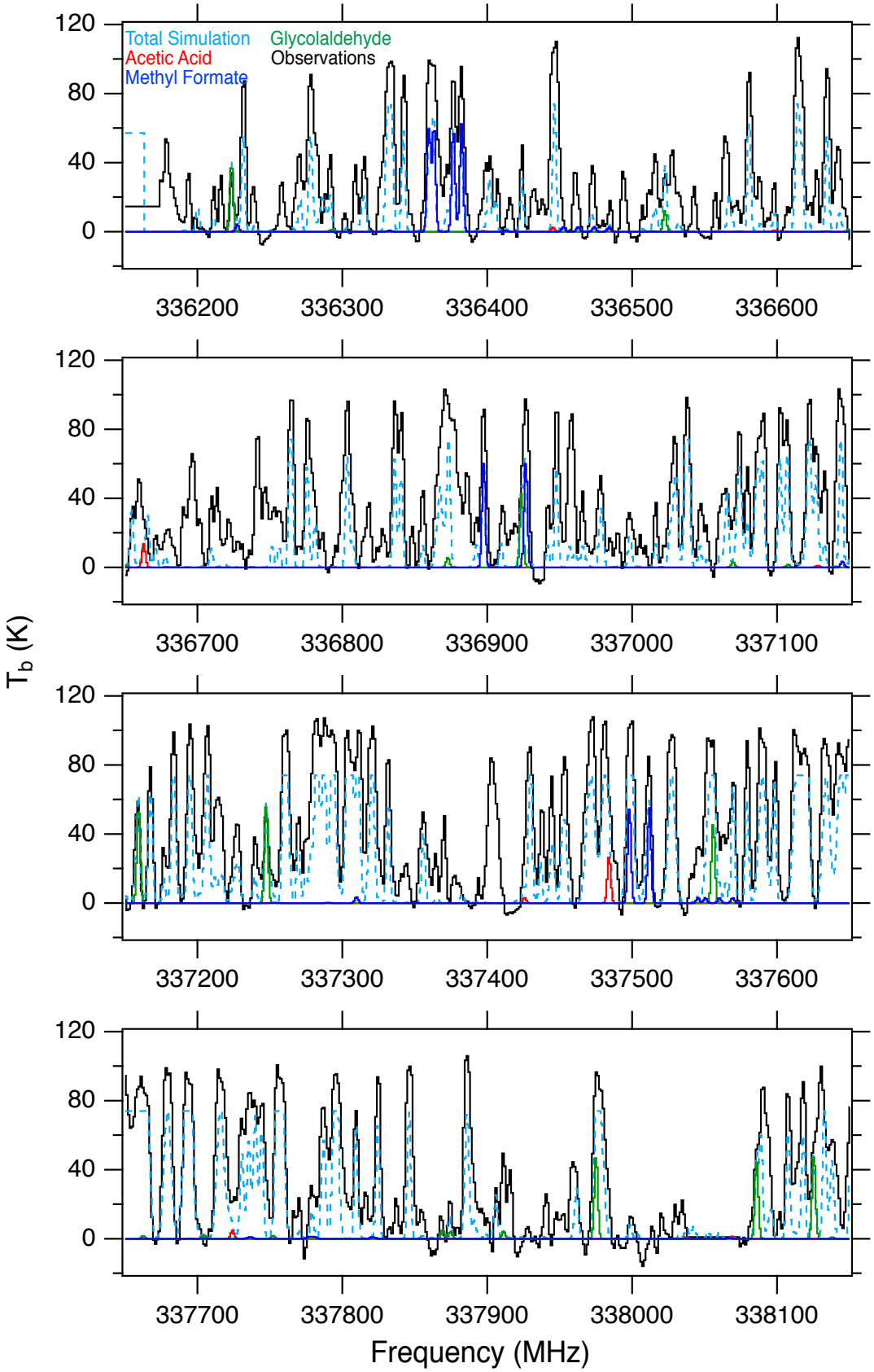

Figure A5. The simulated spectra for methyl formate, acetic acid, and glycolaldehyde are overlaid on the observed spectrum for MM1. The total simulation is also presented. For parameters on each of the fits refer to Table 3.

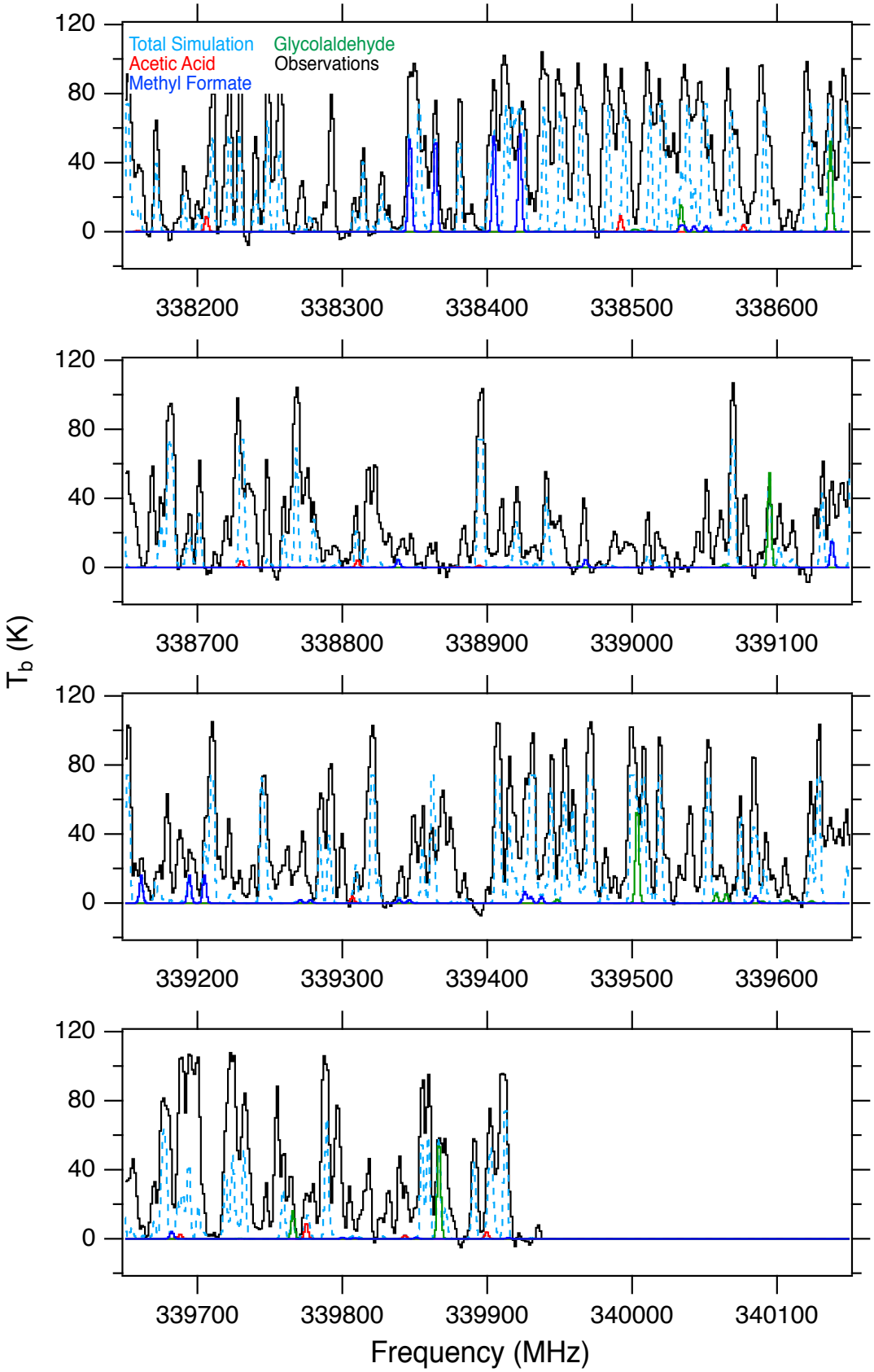

Figure A6. The simulated spectra for methyl formate, acetic acid, and glycolaldehyde are overlaid on the observed spectrum for MM1. The total simulation is also presented. For parameters on each of the fits refer to Table 3.

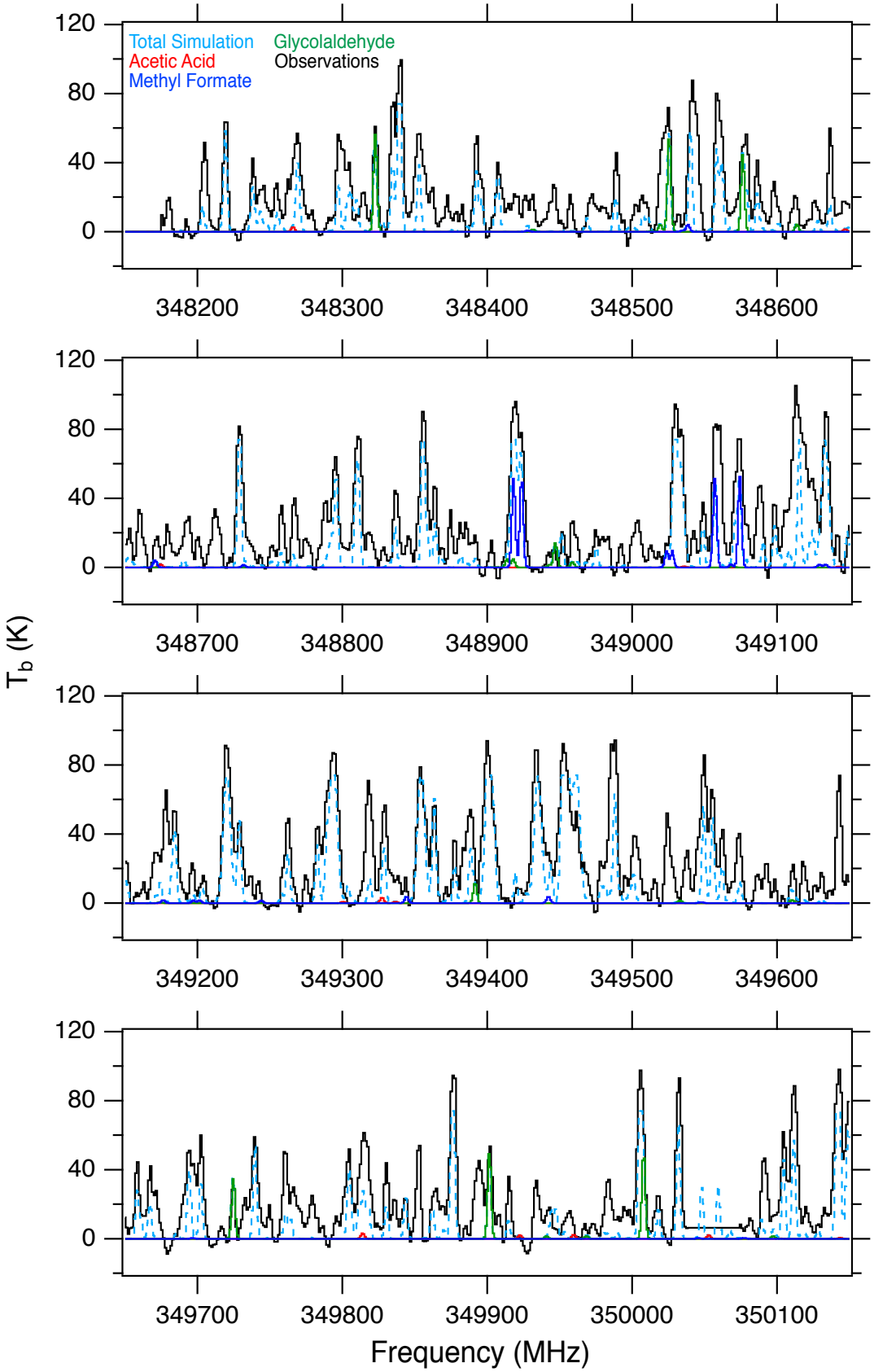

Figure A7. The simulated spectra for methyl formate, acetic acid, and glycolaldehyde are overlaid on the observed spectrum for MM1. The total simulation is also presented. For parameters on each of the fits refer to Table 3.

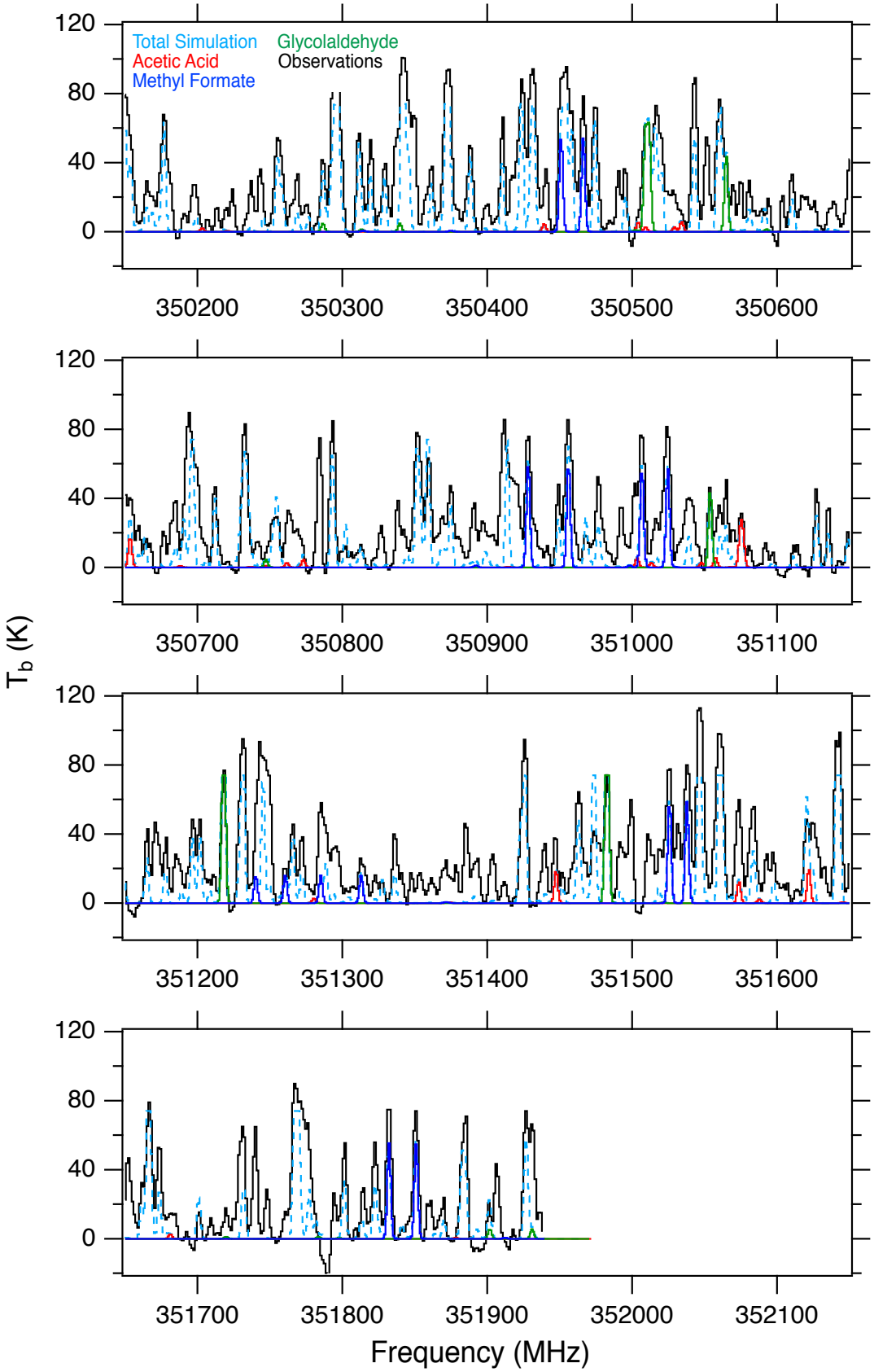

Figure A8. The simulated spectra for methyl formate, acetic acid, and glycolaldehyde are overlaid on the observed spectrum for MM1. The total simulation is also presented. For parameters on each of the fits refer to Table 3.

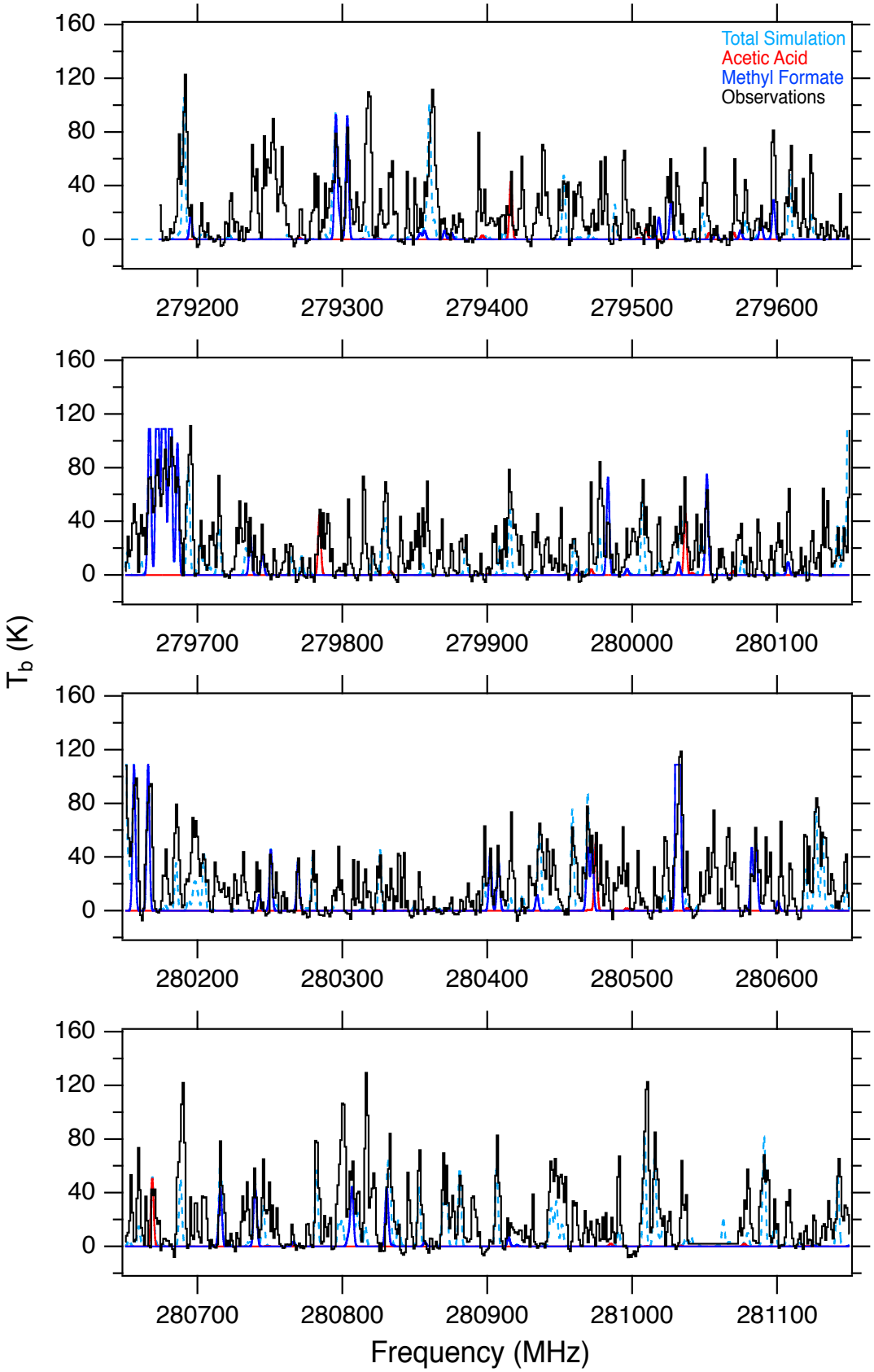

Figure A9. The simulated spectra for methyl formate, acetic acid, and glycolaldehyde are overlaid on the observed spectrum for MM2. The total simulation is also presented. For parameters on each of the fits refer to Table 3.

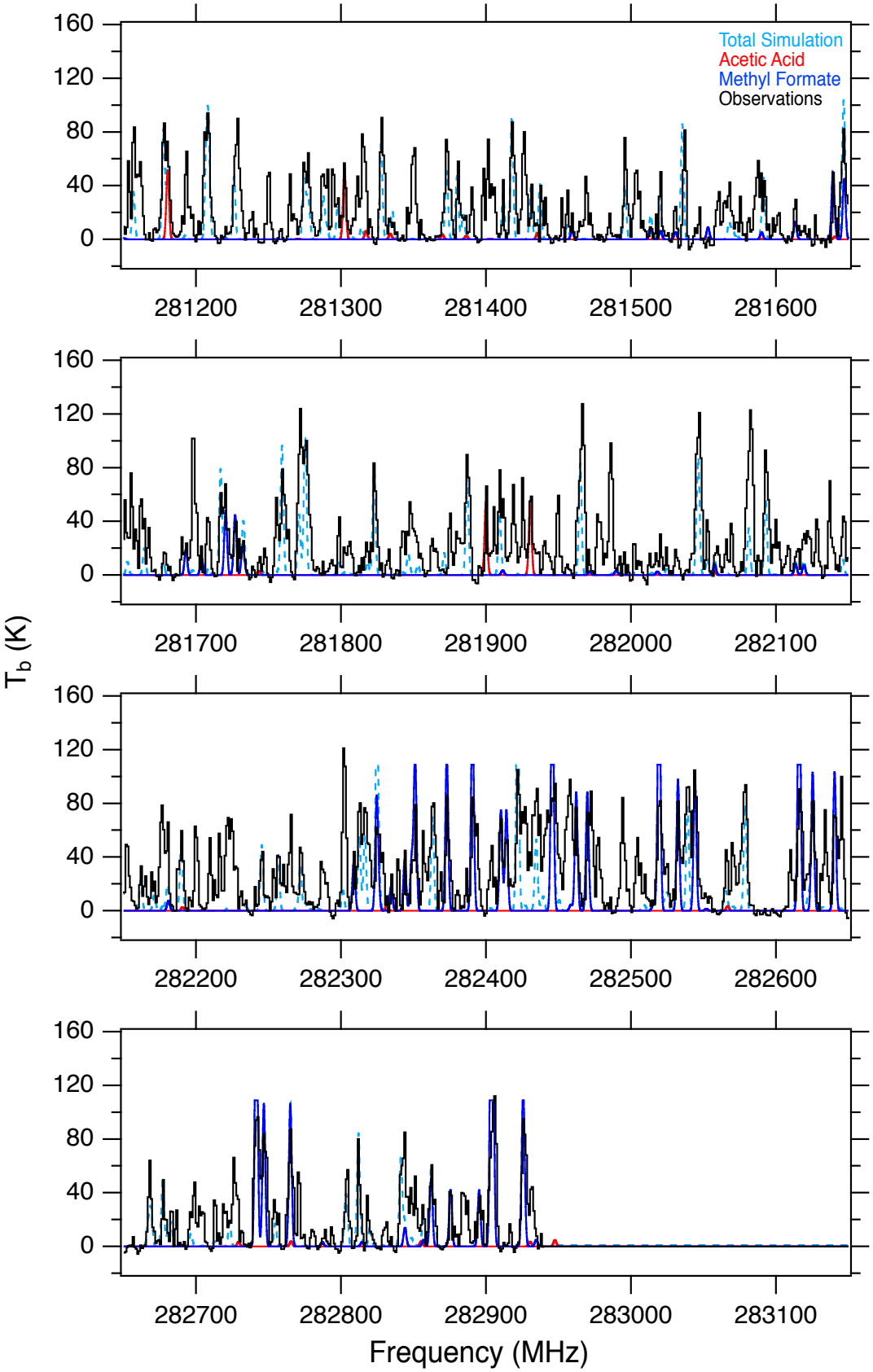

Figure A10. The simulated spectra for methyl formate, acetic acid, and glycolaldehyde are overlaid on the observed spectrum for MM2. The total simulation is also presented. For parameters on each of the fits refer to Table 3.

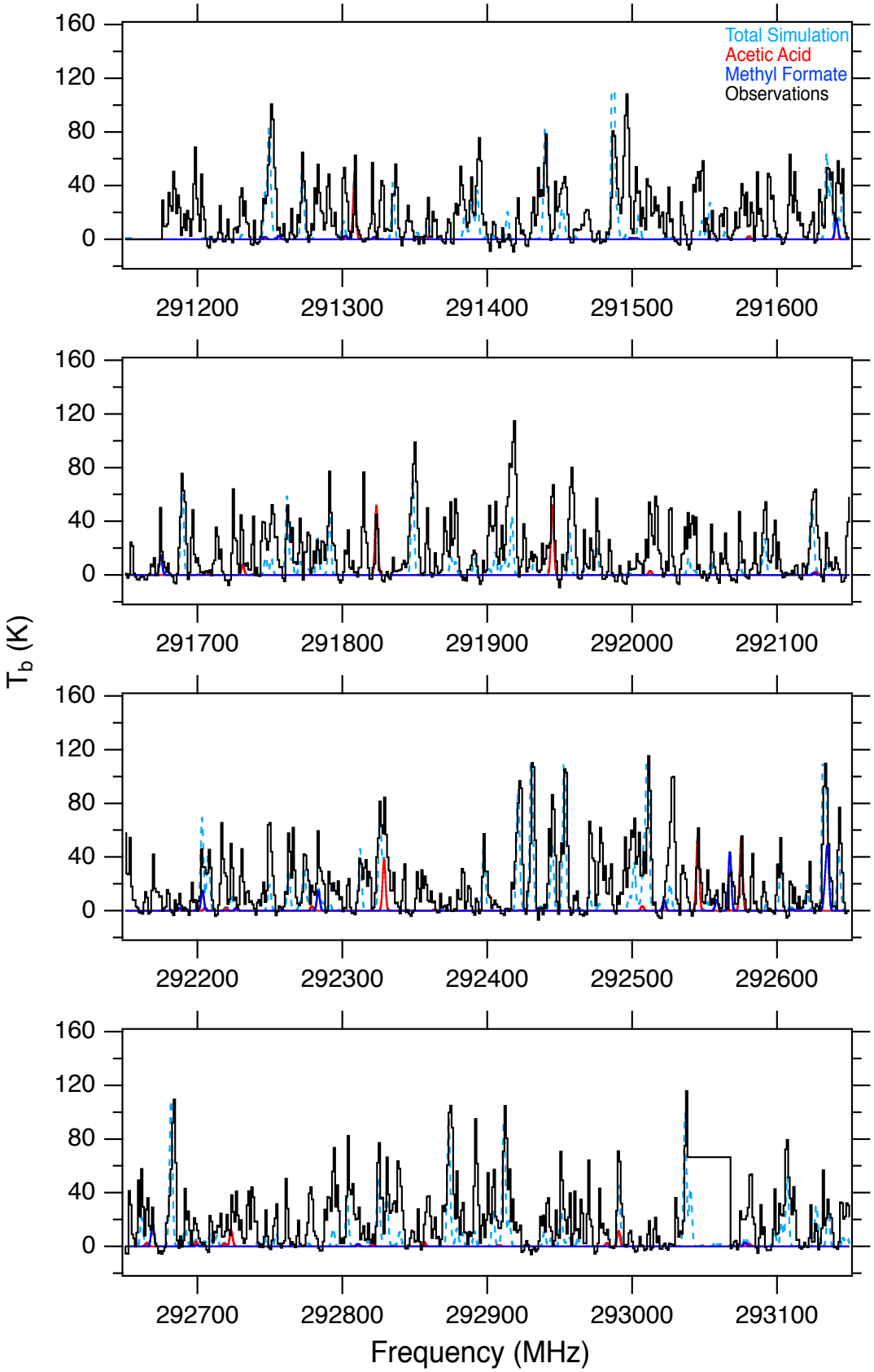

Figure A11. The simulated spectra for methyl formate, acetic acid, and glycolaldehyde are overlaid on the observed spectrum for MM2. The total simulation is also presented. For parameters on each of the fits refer to Table 3.

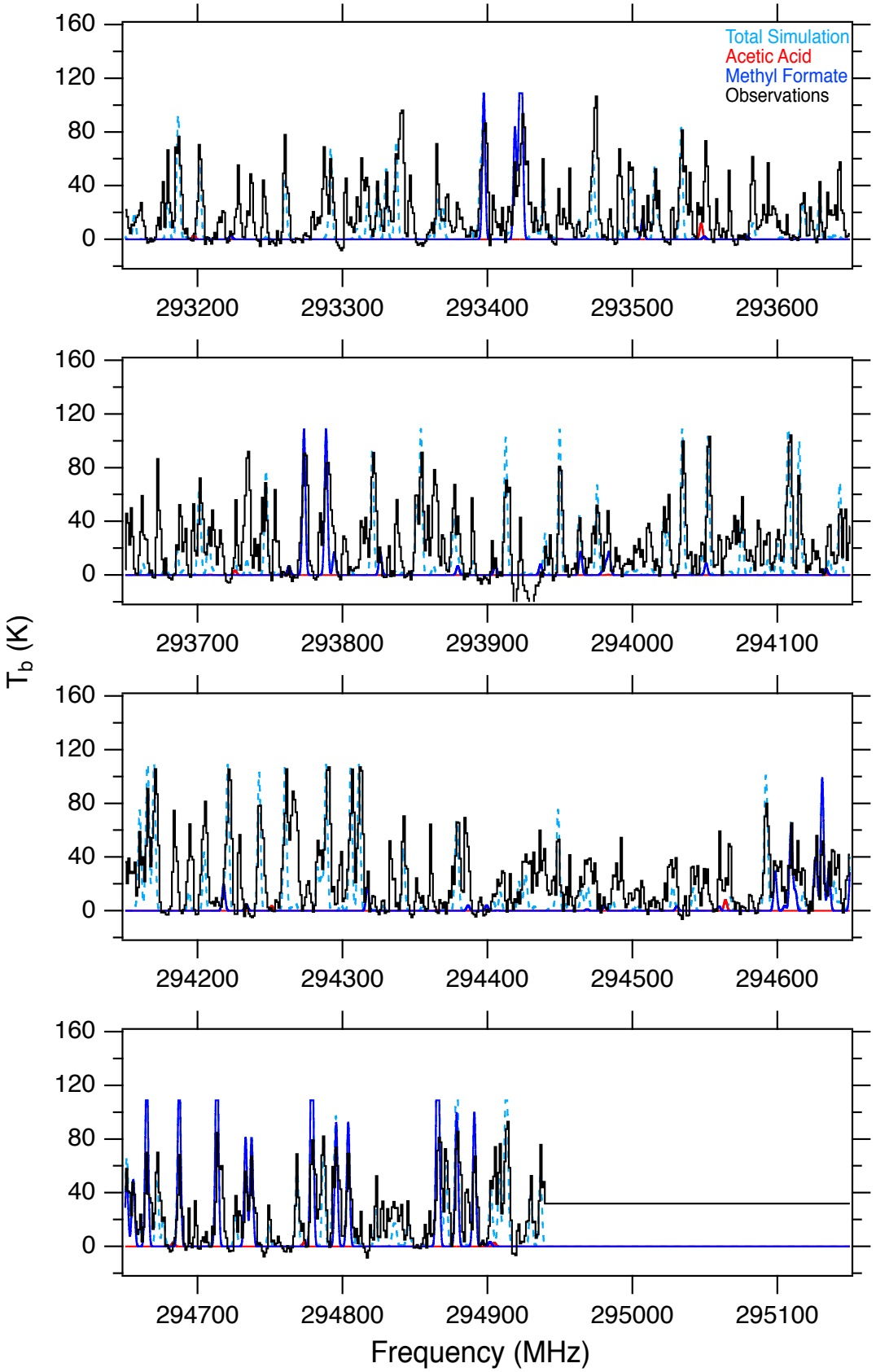

Figure A12. The simulated spectra for methyl formate, acetic acid, and glycolaldehyde are overlaid on the observed spectrum for MM2. The total simulation is also presented. For parameters on each of the fits refer to Table 3.

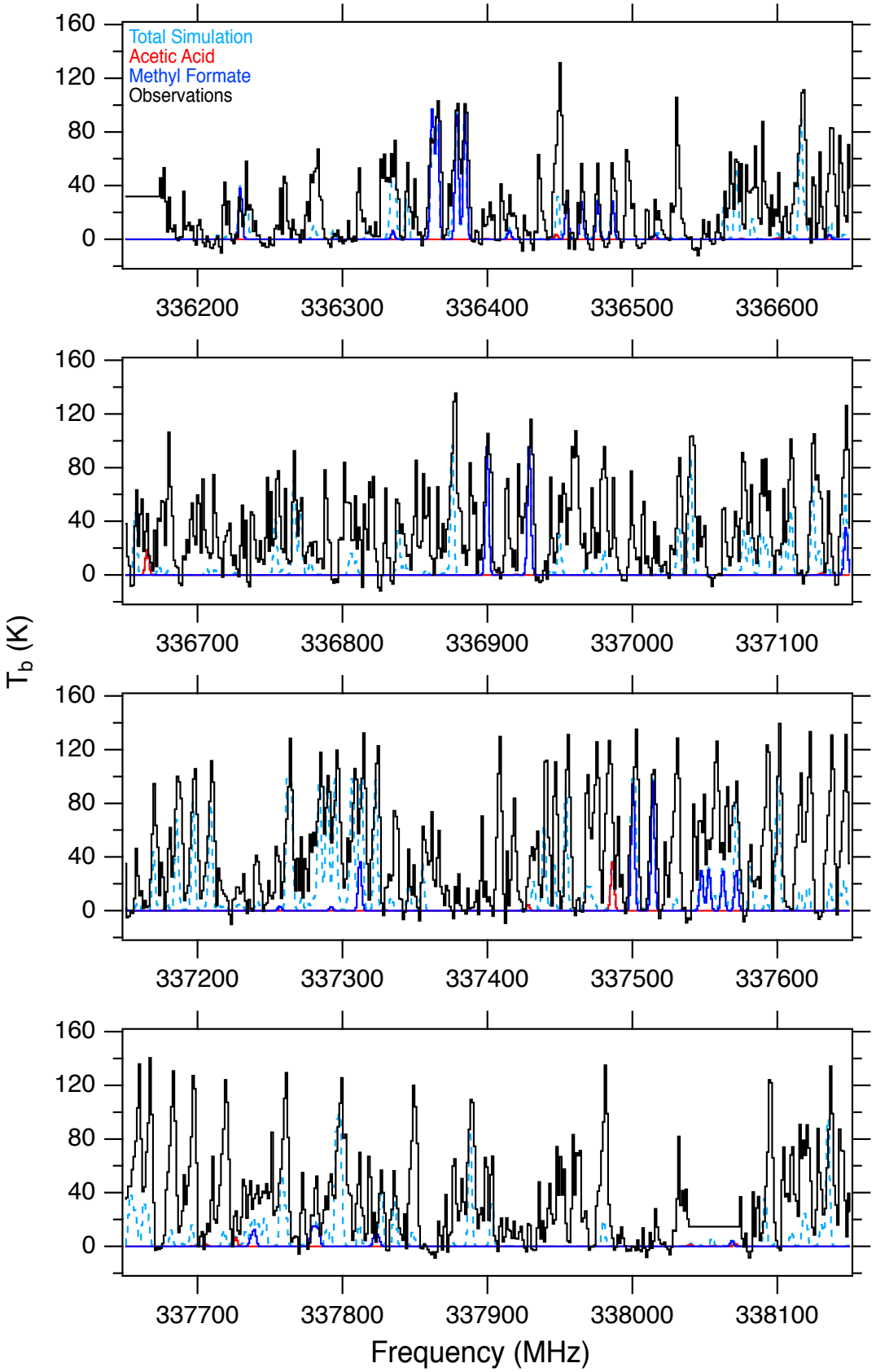

Figure A13. The simulated spectra for methyl formate, acetic acid, and glycolaldehyde are overlaid on the observed spectrum for MM2. The total simulation is also presented. For parameters on each of the fits refer to Table 3.

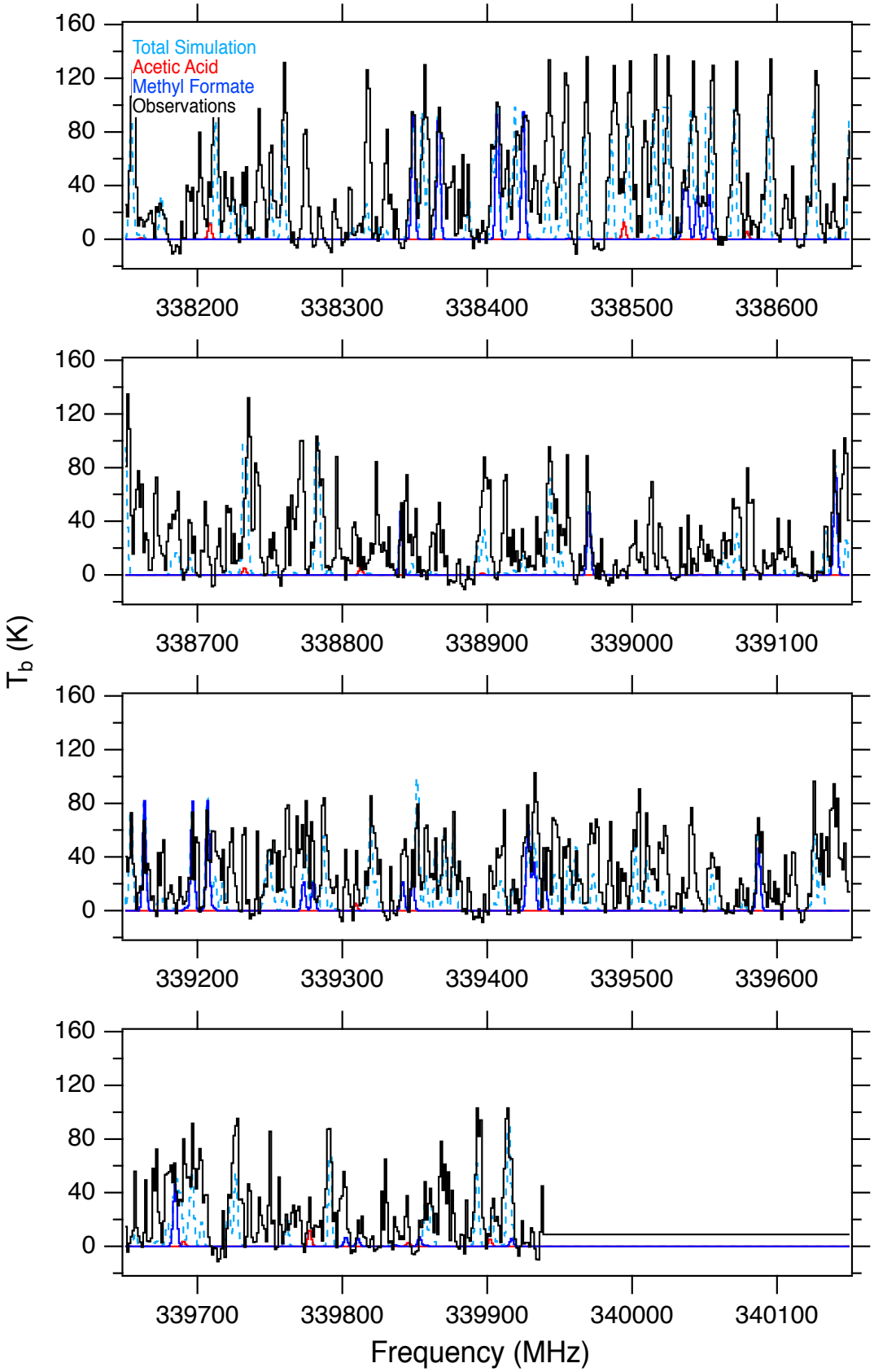

Figure A14. The simulated spectra for methyl formate, acetic acid, and glycolaldehyde are overlaid on the observed spectrum for MM2. The total simulation is also presented. For parameters on each of the fits refer to Table 3.

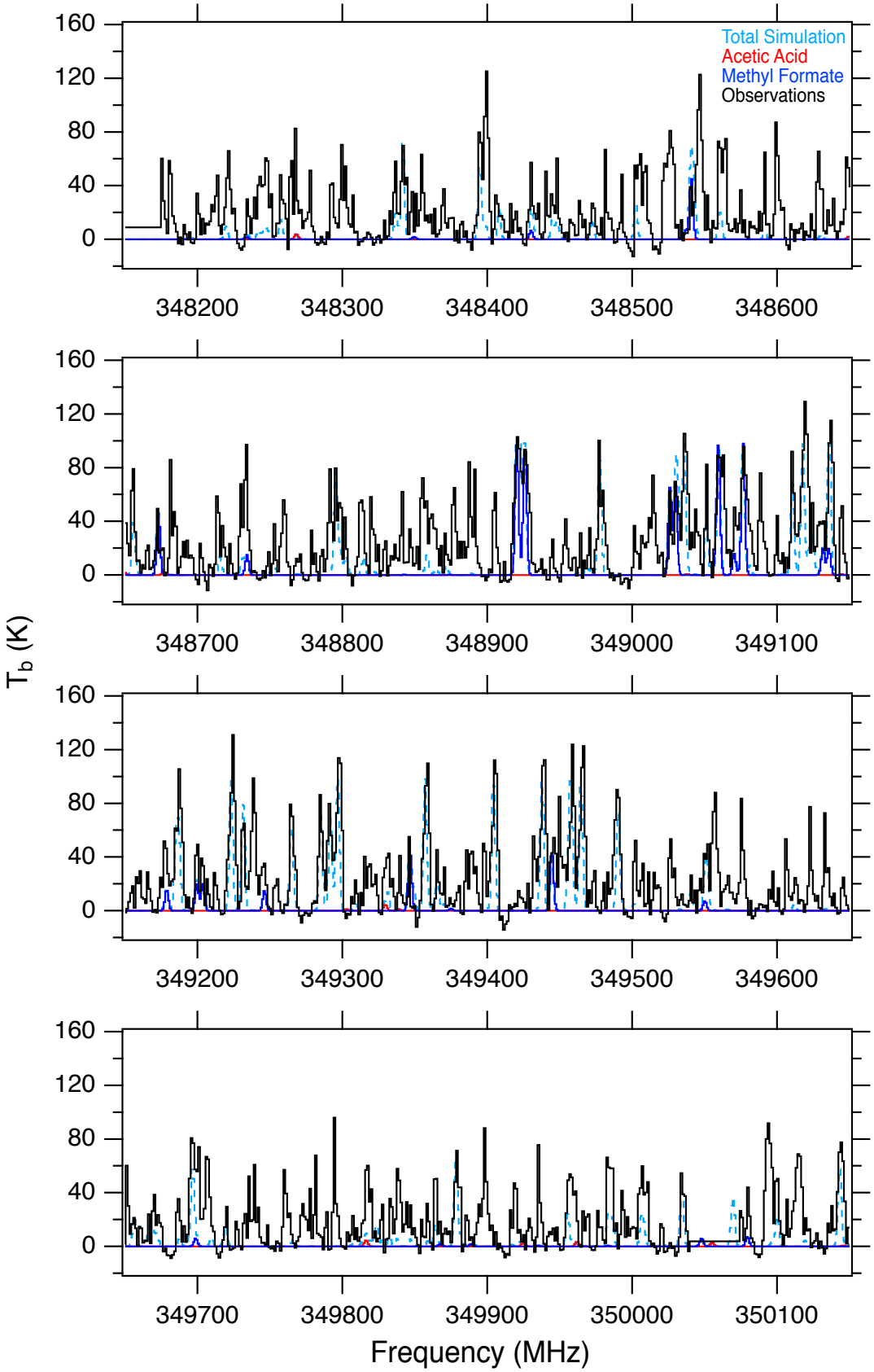

Figure A15. The simulated spectra for methyl formate, acetic acid, and glycolaldehyde are overlaid on the observed spectrum for MM2. The total simulation is also presented. For parameters on each of the fits refer to Table 3.

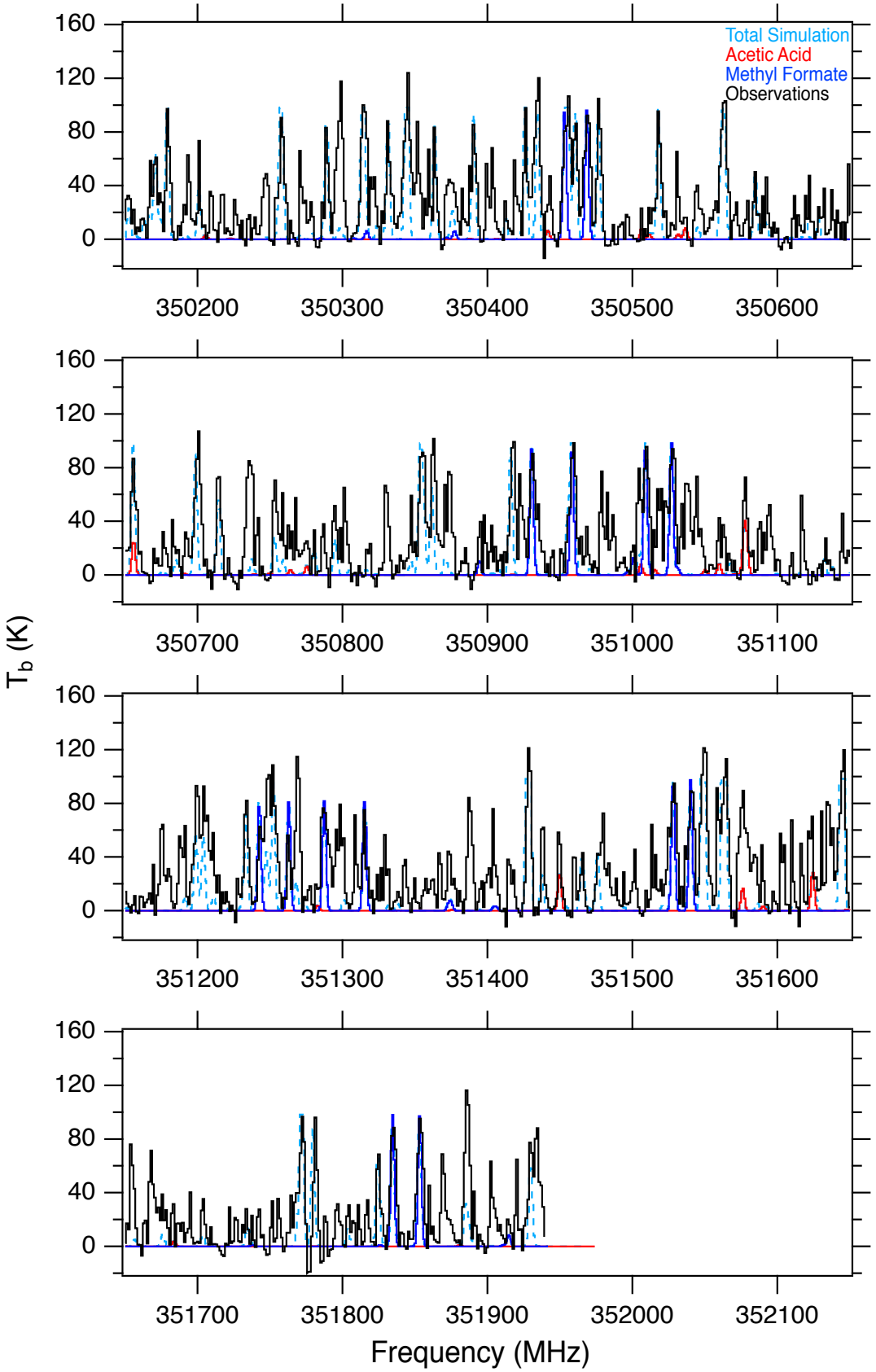

Figure A16. The simulated spectra for methyl formate, acetic acid, and glycolaldehyde are overlaid on the observed spectrum for MM2. The total simulation is also presented. For parameters on each of the fits refer to Table 3.